Size-selective analyte detection with a Young interferometer sensor using multiple wavelengths

Harmen K. P. Mulder,[1,*] Christian Blum,[1] Vinod Subramaniam,[1,2] and Johannes. S. Kanger[1]

[1]*Nanobiophysics Group, MESA + Institute for Nanotechnology, MIRA Institute for Biomedical Technology and Technical Medicine, University of Twente, PO Box 217, 7500 AE Enschede, The Netherlands*
[2]*Nanoscale Biophysics, FOM Institute AMOLF, Science Park 104, Amsterdam, The Netherlands*
[*]*h.k.p.mulder@utwente.nl*

Abstract: We present a method to discriminate between analytes based on their size using multiple wavelengths in a Young interferometer. We measured the response of two wavelengths when adding 85 nm beads (representing specific binding), protein A (representing non-specific binding) and D-glucose (inducing a bulk change) to our sensor. Next, the measurements are analysed using a approach based on theoretical analysis, and a ratio-based analysis approach to discriminate between bulk changes and the binding of the different sized substances. Moreover, we were able to discriminate binding of 85 nm beads from binding of protein A (~2 nm) in a blind experiment using the ratio-based approach. This can for example be used to discriminate specific analyte binding of larger particles from non-specific binding of smaller particles. Therefore, we believe that by adding size-selectivity we can strongly improve the performance of the Young interferometer sensor and integrated optical interferometric sensors in general.

OCIS codes: (120.3180) Interferometry; (130.0130) Integrated optics; (130.6010) Sensors.

References and links

1. K. Cottier, M. Wiki, G. Voirin, H. Gao, and R. E. Kunz, "Label-free highly sensitive detection of (small) molecules by wavelength interrogation of integrated optical chips," Sens. Actuators B Chem. **91**(1-3), 241–251 (2003).
2. G. D. Kim, G. S. Son, H. S. Lee, K. D. Kim, and S. S. Lee, "Integrated photonic glucose biosensor using a vertically coupled microring resonator in polymers," Opt. Commun. **281**(18), 4644–4647 (2008).
3. M. Iqbal, M. A. Gleeson, B. Spaugh, F. Tybor, W. G. Gunn, M. Hochberg, T. Baehr-Jones, R. C. Bailey, and L. C. Gunn, "Label-free biosensor arrays based on silicon ring resonators and high-speed optical scanning instrumentation," IEEE J. Sel. Top. Quantum Electron. **16**(3), 654–661 (2010).
4. H. Zhu, I. M. White, J. D. Suter, and X. Fan, "Phage-based label-free biomolecule detection in an opto-fluidic ring resonator," Biosens. Bioelectron. **24**(3), 461–466 (2008).
5. N. Skivesen, A. Têtu, M. Kristensen, J. Kjems, L. H. Frandsen, and P. I. Borel, "Photonic-crystal waveguide biosensor," Opt. Express **15**(6), 3169–3176 (2007).
6. S. C. Buswell, V. A. Wright, J. M. Buriak, V. Van, and S. Evoy, "Specific detection of proteins using photonic crystal waveguides," Opt. Express **16**(20), 15949–15957 (2008).
7. A. Brandenburg, R. Krauter, C. Künzel, M. Stefan, and H. Schulte, "Interferometric sensor for detection of surface-bound bioreactions," Appl. Opt. **39**(34), 6396–6405 (2000).
8. C. Stamm, R. Dangel, and W. Lukosz, "Biosensing with the integrated-optical difference interferometer: dual-wavelength operation," Opt. Commun. **153**(4-6), 347–359 (1998).
9. K. Schmitt, B. Schirmer, C. Hoffmann, A. Brandenburg, and P. Meyrueis, "Interferometric biosensor based on planar optical waveguide sensor chips for label-free detection of surface bound bioreactions," Biosens. Bioelectron. **22**(11), 2591–2597 (2007).
10. A. Ymeti, J. S. Kanger, R. Wijn, P. V. Lambeck, and J. Greve, "Development of a multichannel integrated interferometer immunosensor," Sens. Actuators B Chem. **83**(1-3), 1–7 (2002).

#257853 Received 5 Feb 2016; revised 14 Mar 2016; accepted 15 Mar 2016; published 12 Apr 2016

11. R. G. Heideman and P. V. Lambeck, "Remote opto-chemical sensing with extreme sensitivity: design, fabrication and performance of a pigtailed integrated optical phase-modulated Mach–Zehnder interferometer system," Sens. Actuators B Chem. **61**(1-3), 100–127 (1999).
12. C. Worth, B. B. Goldberg, M. Ruane, and M. S. Unlu, "Surface desensitization of polarimetric waveguide interferometers," IEEE J. Sel. Top. Quantum Electron. **7**(6), 874–877 (2001).
13. G. H. Cross, A. A. Reeves, S. Brand, J. F. Popplewell, L. L. Peel, M. J. Swann, and N. J. Freeman, "A new quantitative optical biosensor for protein characterisation," Biosens. Bioelectron. **19**(4), 383–390 (2003).
14. R. A. Abram and S. Brand, "Some theory of a dual-polarization interferometer for sensor applications," J. Phys. D Appl. Phys. **48**(12), 125101 (2015).
15. H. K. P. Mulder, A. Ymeti, V. Subramaniam, and J. S. Kanger, "Size-selective detection in integrated optical interferometric biosensors," Opt. Express **20**(19), 20934–20950 (2012).
16. P. Kozma, F. Kehl, E. Ehrentreich-Förster, C. Stamm, and F. F. Bier, "Integrated planar optical waveguide interferometer biosensors: a comparative review," Biosens. Bioelectron. **58**, 287–307 (2014).
17. S. Ohnishi, M. Murata, and M. Hato, "Correlation between surface morphology and surface forces of protein A adsorbed on mica," Biophys. J. **74**(1), 455–465 (1998).
18. M. C. Coen, R. Lehmann, P. Gröning, M. Bielmann, C. Galli, and L. Schlapbach, "Adsorption and bioactivity of protein A on silicon surfaces studied by AFM and XPS," J. Colloid Interface Sci. **233**(2), 180–189 (2001).

1. Introduction

Integrated optical (IO) sensors are demonstrated to be a good analysis and detection tool for biosensing, mainly because of their high sensitivity, and their ability to measure real-time and label-free. Examples of IO sensors are grating couplers [1], resonant optical microcavity sensors [2–4], photonic crystal waveguide sensors [5,6] and interferometric sensors [7–11]. Interferometric biosensors use the evanescent field to detect refractive index (RI) changes induced by analyte binding. Extremely high RI sensitivities ($\sim 10^{-8}$ refractive index units (RIU)) are reported with interferometric sensors like the Mach-Zehnder interferometer [11] and the Young interferometer (YI) [9,10]. However, it is often not possible to fully use the high sensitivity capabilities of the sensor, because any RI change within the evanescent field will contribute to the measured signal. Next to the specific signal arising from specific binding of the analyte, signals originate from non-specific bound particles and RI changes in the fluid covering the waveguide (bulk). To discriminate specific binding from non-specific binding, selective chemical binding techniques are used in combination with washing steps. Differential measurements are used to cancel out bulk changes. Nevertheless, successful application of IO biosensors is still hampered by non-specificity due to bulk effects or non-specific adhesion. Therefore, a method was developed to reduce the contribution of non-specific binding to the measured signal [12]. The response to non-specific binding was reduced by a factor of hundred or more by tuning the evanescent fields of two different polarization modes such that the first 20-30 nm of the evanescent field were desensitized to reduce the contribution of non-specific binding. However, any RI change in this layer cannot be detected, resulting also in a reduction of the contribution due to specific binding. Moreover, a dual wavelength operation of an IO difference interferometer was used to distinguish binding of molecules from bulk changes or temperature changes [8]. Alternatively, dual polarization interferometry can be used to determine both the thickness and density (RI) of an adlayer [13,14]. Finally, we presented a theoretical description of a method called size-selective detection which can be used to discriminate between RI changes from binding of different sized particles and bulk changes (e.g. due to temperature changes) simultaneously [15]. Our theoretical analysis showed that it is possible to determine RI changes from multiple layers above the surface waveguide by measuring RI changes in the evanescent field at multiple wavelengths. Here, we present the experimental realisation of this theoretical analysis. We also present a new, more pragmatic, analysis approach which can be used to discriminate binding of particles from bulk changes and distinguish binding between different sized particles.

#257853 Received 5 Feb 2016; revised 14 Mar 2016; accepted 15 Mar 2016; published 12 Apr 2016

2. Materials and methods

2.1 Young interferometer with multiple wavelengths

For the general theory of the working of the YI and how it can be used to determine multiple RI changes based on measurements with multiple wavelengths we refer to our theoretical article (Mulder et al. 2012). That article also showed that adding size-selectivity negatively affects the precision of the measured RI change. However, using three wavelengths to discriminate between RI changes at three different layers within the evanescent field and assuming a phase precision of 10^{-4} fringes and current waveguide specifications, the retained theoretical sensitivity is $1x10^{-6}$ RIU corresponding to 0.8 pg/mm^2, which is still comparable to the detection limits of other existing methods [16]. In the measurements shown in this contribution we discriminate between two substances of different sizes inducing a RI change by measuring the effective refractive index change ΔN_{eff} at two wavelengths (457 and 660 nm). Measurements with three wavelengths also showed that we could discriminate between three substances (see Appendix C), however results of Δn became very noise because of enhancement of artefacts due to boundary effects of the shifting interference pattern (see Noise, drift and artefacts in measurements). For a successful application of these analysis approaches used to determine three independent Δn's, artefacts and drift in ΔN_{eff} should be reduced significantly. All the experimental details about the setup are given in Appendix A.

2.2 Measurement protocol

When a substance (with a different RI than the initial solution) is added to the evanescent field in the sensing window, this results in a RI change Δn resulting in a ΔN_{eff}. This ΔN_{eff} is determined by reading out the $\Delta\varphi$ (in fringes) and multiplying it by the wavelength of the light source and dividing it by the sensing window length of the chip. This is done for the three wavelengths such that a ΔN_{eff} is determined for each wavelength. The substances that we measure with the sensor are 85 nm carboxylated polystyrene beads which bind to the sensor surface (representing specific binding of e.g. viruses which approximately this size), protein A (representing non-specific binding) which also binds to the sensor surface but is smaller (≈2 nm [17, 18]) and D-glucose which hardly binds to the sensor surface but induces a bulk change. These substances induce Δn's at different places within the evanescent field and can therefore be discriminate from each other. In this case we discriminate between substances of different materials, but it is also possible to discriminate between substances of the same material as long as they are different in size. All the measurements are done using a 1x phosphate buffered saline (PBS) buffer to which the different samples were added. The measurements start with a baseline of approximately 400 s to determine the drift of ΔN_{eff} signal (can be caused e.g. by temperature fluctuations causing relative movement between chip and CCD camera or causing directly a Δn at the sensing windows) which results in drift in Δn (see Appendix E). Next, the measurements continue with a characterization step, containing an addition of 6.16 mg/ml D-glucose for 500 s to the PBS, which can be used to verify that the sensor responds as expected or to fit a theoretical model by changing waveguide parameters such that the determined curves of Δn fulfil the expectations.

3. Theory

Usually, a YI is used to determine a ΔN_{eff} at a single wavelength. Consequently, an average Δn is determined, based on any Δn in the whole evanescent field. Measuring the ΔN_{eff} at multiple different wavelengths enables discrimination between multiple different Δn's. Here, we shortly describe two analysis approaches which can be used for this: an approach based on

#257853 Received 5 Feb 2016; revised 14 Mar 2016; accepted 15 Mar 2016; published 12 Apr 2016

theoretical analysis and a ratio-based analysis approach. A more detailed description of the ratio-based approach can be found in Appendix B.

3.1 Approach based on theoretical analysis

Determining the ΔN_{eff} at two different wavelengths, enables the discrimination between Δn 's originating from two arbitrarily chosen layers within the evanescent field [15], using the following equation:

$$\overline{\Delta n_l} = \overline{\overline{S}}^{-1} \cdot \overline{\Delta N_{eff}}, \tag{1}$$

where the element $\Delta n_{l,j}$ of vector $\overline{\Delta n_l}$ is the RI change in the j^{th} layer (index l stands for layer), the elements $S_{i,j} = \left(\partial N_{eff,\lambda_i} / \partial n\right)_j$ of matrix $\overline{\overline{S}}$ are the theoretical sensitivity coefficients, which are the derivatives of N_{eff} at the i^{th} wavelength with respect to n occurring in the j^{th} layer and the element $\Delta N_{eff,i}$ of vector $\overline{\Delta N_{eff}}$ is the ΔN_{eff} at the i^{th} wavelength. The sensitivity coefficients are determined by the structure of the waveguide (core thickness and RIs of the various layers of the waveguide), the wavelengths, the polarization and two arbitrarily chosen layers (within the evanescent field). The $\overline{\Delta n_l}$ can be determined by measuring $\overline{\Delta N_{eff}}$ and multiplying this by the inverse of matrix $\overline{\overline{S}}$. A homogeneous Δn_l per layer is determined and therefore this method is less suitable for situations where Δn 's are induced in the same layer by different substances. However, assuming a low concentration of analytes, for example bulk effects can be cancelled out by subtraction of Δn determined from multiple layers to finally arrive at an analyte concentration [15]. Nevertheless, this method requires tuning of many parameters to determine the correct values for the sensitivity coefficients that are required to determine the absolute value of Δn. Hence, this method is exact but in practice difficult to implement because of the many parameters that have to be tuned. This approach also requires more input than actually required, so therefore we developed a much more practical and easy to use ratio-based approach.

3.2 Ratio-based approach

Here, we present the ratio-based analysis approach which uses the ratios of ΔN_{eff} at multiple wavelengths, caused by Δn 's originating from different substances Δn_s. Each substance with a different size which causes a Δn_s in the evanescent field results in different ΔN_{eff} 's for each wavelength because of the different electric field distributions of the respective wavelengths. The ratio of the ΔN_{eff} measured at two different wavelengths λ_k and λ_l, induced by a substance s_m, is defined as:

$$R^{s_m}_{\lambda_k/\lambda_l} = \frac{\Delta N^{s_m}_{eff,\lambda_k}}{\Delta N^{s_m}_{eff,\lambda_l}}. \tag{2}$$

RI changes of multiple substances inducing different ratios can be discriminated from each other as a function of the measured ratios using (see Appendix B information for derivation):

$$\overline{\Delta n_s} = \overline{\overline{\Theta}}^{-1} \cdot \overline{\overline{R}}^{-1} \cdot \overline{\Delta N_{eff}}, \tag{3}$$

#257853 Received 5 Feb 2016; revised 14 Mar 2016; accepted 15 Mar 2016; published 12 Apr 2016

where vector $\overline{\Delta n_s}$ is composed of the elements Δn_{s_m} (the refractive index change caused by substance s_m), the vector $\overline{\Delta N_{eff}}$ is composed of the elements $\Delta N_{\mathrm{eff},\lambda_k}$, where $\overline{\overline{\Theta}}$ is a matrix with theoretical sensitivity coefficients of which the elements are given by $\theta_{k,m} = \partial N_{eff,\lambda_k} / \partial n_{s_m} \; \forall \; k = m$ and $\theta_{k,m} = 0 \; \forall \; k \neq m$, and the coefficients of matrix $\overline{\overline{R}}$ are given by $r_{k,m} = R^{s_m}_{\lambda_k/\lambda_m}$. The experimental procedure is now as follows. First a characterization step is required to determine matrix $\overline{\overline{R}}$ by measuring the response of the sensor for each individual substance. The matrix $\overline{\overline{\Theta}}^{-1}$ can be regarded as a scaling matrix that allows to get absolute values of $\overline{\Delta n_s}$. When the coefficients of this matrix are unknown, $\theta_{k,m} \; \forall \; k = m$ can be set as 1 such that $\overline{\overline{\Theta}}^{-1}$ becomes the identity matrix, which means that $\overline{\Delta n_s}$ is fully determined by the measured ratios $R^{s_m}_{\lambda_k/\lambda_m}$. Without the scaling it is possible to compare the unscaled Δn_{s_m} with Δn_{s_m} of a different measurement. However, the amplitude of Δn_{s_m} should not be compared with Δn_{s_n} as scaling is required. Now that we know the matrices of Eq. (3), we can use this equation. for analysis of a real experiment in which we add multiple substances simultaneously to the sensor to find the contribution of each substance independently.

An advantage of the ratio-based method is that direct discrimination between different substances is possible, also when Δn_s's occur in same layer in the evanescent field, as long as the ratios in wavelengths are different from each other and as long as the substances do not influence each other's response of the sensor. The analysis of two substances which induce a Δn_s is relatively easy as only two ratios are determinable parameters which determine the shape of the signal of $\overline{\Delta n_s}$ over time. For three substances inducing a Δn_s, already six ratios need to be determined, illustrating the rapidly increasing complexity when increasing the number of distinguishable substances inducing a Δn_s. However, these ratios can be determined independently for each substance to discriminating these substances from each other.

The absolute value of $\overline{\Delta n_s}$ can be determined by combining the ratio-based approach with the theoretical model used for the approach based on the theoretical analysis. In this way $\overline{\overline{\Theta}}^{-1}$ can be determined. However, this requires again tuning of a lot of parameters. Therefore, it might be easier to determine scaling parameters for $\overline{\Delta n_s}$ using calibration experiments, which are usually also carried out by a single wavelength. Alternatively, this method can also be used as a quick screener, providing only a yes or no answer on the presence of the analyte and which therefore does not require knowing the absolute values of $\overline{\Delta n_s}$.

4. Results and discussion

First, we present the measured ratios $R^{s_m}_{\lambda_k/\lambda_l}$ for the individual substances which are used for the ratio-based approach to discriminate between these different-sized substances. Second, we present measurements in which two substances simultaneously induced a Δn and the corresponding results obtained from both the approach based on theoretical analysis and the ratio-based analysis approach. Third, we demonstrate the power of the ratio-based approach in a blind experiment were the binding of 85 nm beads was discriminated from binding of protein A.

#257853 Received 5 Feb 2016; revised 14 Mar 2016; accepted 15 Mar 2016; published 12 Apr 2016

4.1 Ratios of individual substances

Here, we present the measured ratios of ΔN_{eff} measured at different wavelengths for each individual substance which are used for the ratio-based approach in order to discriminate between these substances in the measurements presented in the next sections. We measured the ratios for two different wavelengths (λ_1 = 457 nm and λ_2 = 660 nm), and three different substances: 85 nm carboxylated polystyrene beads ($R_{660/457}^{\text{beads}}$ = 0.918 ± 0.045), protein A ($R_{660/457}^{\text{protein}}$ = 0.680 ± 0.022) and D-glucose ($R_{660/457}^{\text{glucose}}$ = 1.218 ± 0.016). The error margins of the ratios are determined by twice the standard deviation (95% confidence interval) of the measured ratios from different experiments. A more detailed description of how these ratios are determined is found in the Appendix B. The spread in the measured ratios might be caused by artefacts in the measurements (see section 4.4) or slightly different sensor surface properties from run-to-run due to unequal cleaning which can result in changes in binding as we use non-specific binding of the protein A and 85 nm beads. The ratios of the different substances are in principle independent of the substance concentration as long as the resulting surface concentrations are much smaller than a full monolayer coverage. When substances bind on top of each other this will result in a different ratio and therefore the proposed method is not valid anymore.

4.2 Discrimination between two different-sized substances

In this section we present measurements where two of the three named different-sized substances (protein A, 85 nm beads and D-glucose which induces a homogeneous Δn in the whole evanescent field of a few hundreds of nanometres) are discriminated from each other. First, 6.16 mg/ml D-glucose and 2.0 µg/ml protein A were added simultaneously to the sensor (see Fig. 1(a)) and ΔN_{eff} is measured at λ_1 = 457 nm and λ_2 = 660 nm. As a characterization step 6.16 mg/ml D-glucose only was added to the sensor, which results in an increase of the ΔN_{eff} as D-glucose has a higher n than PBS. As expected, the ΔN_{eff} is the highest at λ_2 as it is more sensitive to bulk changes (D-glucose does hardly bind to the surface) compared to λ_1. After applying a washing step, the ΔN_{eff} comes back to zero as the D-glucose bulk solution is completely replaced by PBS. After simultaneously adding D-glucose and protein A the ΔN_{eff} increases again differently at λ_1 compared to λ_2. For both ΔN_{eff}'s the increase consist of a steep slope due to the bulk effect and a less steep slope due to the binding of the protein A to the surface. After again applying a washing step the signal drops due to the fact that the D-glucose and protein A in the bulk are replaced by PBS. The ΔN_{eff} does not go back to zero as protein A is left at the surface. In this case the ΔN_{eff} at λ_1 is higher than at λ_2 which is expected since shorter wavelengths are more confined to the core of the waveguide and have a relative larger field near the surface compared to the longer wavelengths. Therefore, the shorter wavelengths are more sensitive to changes close to the surface compared to longer wavelengths. Figure 1(d) shows a similar experiment where after addition of only 6.16 mg/ml D-glucose, 6.16 mg/ml D-glucose was added simultaneously with 1.0 µg/ml 85 nm beads. Figure 1(g) shows a similar measurement where after addition of only 6.16 mg/ml D-glucose,1.0 µg/ml protein A was added simultaneously with 2.0 µg/ml 85 nm beads respectively.

#257853 Received 5 Feb 2016; revised 14 Mar 2016; accepted 15 Mar 2016; published 12 Apr 2016

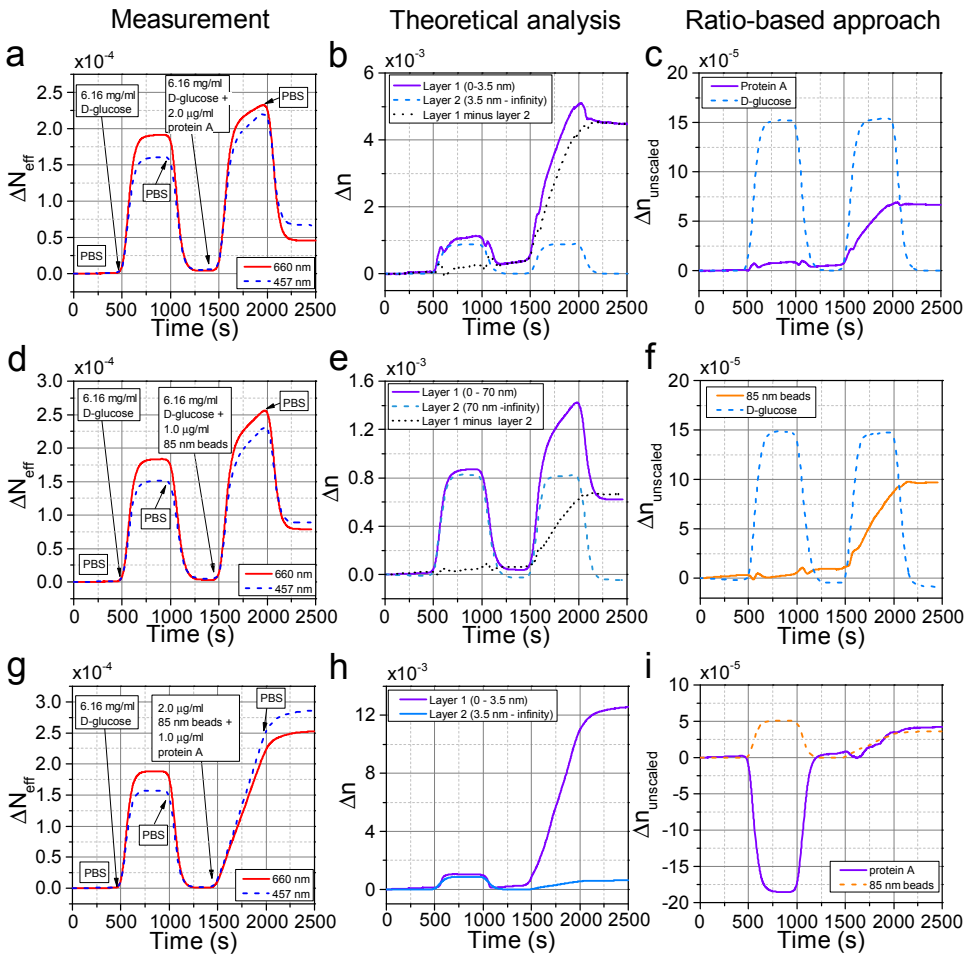

Fig. 1. Two substances discriminated from each other. The ΔN_{eff} measured over time by adding to the sensor surface: a) 85 nm carboxylated polystyrene beads and D-glucose, d) protein A and D-glucose and g) protein A and 85 nm carboxylated polystyrene beads and corresponding determined Δn using the approach based on theoretical analysis (b, e, h) and the ratio-based analysis approach (c, f, i). Corresponding determined Δn using the theoretical and ratio-based analysis method is shown in respectively e) and f).

4.2.1 Protein A and D-glucose

Figure 1(b) shows the Δn corresponding to Fig. 1(a) determined with the approach based on theoretical analysis. Assuming a homogeneous Δn in the whole evanescent field for the D-glucose characterization step, the determined Δn_{l_1} should be the same as Δn_{l_2}, independent of the arbitrarily chosen thickness of the layers. The d_{core}, which determines the theoretical sensitivity coefficients and therefore Δn, can be adjusted such that both Δn's of both layers for the glucose step reach an equal level, independent of the selected layers. The best fit of Δn was achieved by a d_{core} of 61.8 nm. Other waveguide parameters were also tuned to fit the measurement data, but did not give better results. The Δn for the first D-glucose step based on a d_{core} of 61.8 nm is equal to $8.78\text{x}10^{-4}$ RIU, which agrees well with the $8.88\text{x}10^{-4}$ RIU determined from the ΔN_{eff} measured at a single wavelength (660 nm) assuming d_{core} = 61.8 nm.

#257853 Received 5 Feb 2016; revised 14 Mar 2016; accepted 15 Mar 2016; published 12 Apr 2016

Next to the d_{core}, also the layer thickness of the first layer (d_1), of which one can determine a Δn, can be adjusted. Changing d_1 results in a varying end level of Δn_{l_1} and Δn_{l_2} as layer 1 is defined from 0 - d_1 and layer 2 from d_1 - infinity. In the case of simultaneous addition of D-glucose and protein A, the expected end level of Δn_{l_2} after the washing step back to PBS is zero. The layer thickness that provides the expected bulk levels for the experiment with the protein A and D-glucose is 3.5 nm, which is reasonably close to the determined height of an absorbed layer of protein A of approximately 1 nm [18] and 2.5 nm [17]. Assuming low concentrations and bulk changes occurring in both layers, the Δn_{l_2} was subtracted from Δn_{l_1} resulting in a signal which should belong to only the protein A (see black dotted line in Fig. 1(b). The signal belonging to the protein A at the end of the measurement is equal to approximately a seventeenth of a full coverage of protein A.

The determined Δn corresponding to Fig. 1(a) and based on the ratio-based approach is shown in Fig. 1(c). The ratios $R_{660/457}^{\text{protein}}$ and $R_{660/457}^{\text{glucose}}$ that were used for this ratio-based approach are the ratios measured for the individual substances. The $\Delta n_{\text{glucose}}$ fulfils the expectations as the signal goes up when D-glucose was added and comes down to the baseline when applying a washing step. The $\Delta n_{\text{protein}}$ goes up when protein A was added and slowly decreases after applying a washing step, which is probably be caused by partly desorption of the protein A from the sensor surface. However, $\Delta n_{\text{protein}}$ goes also slightly up when D-glucose was added. With an $R_{660/457}^{\text{glucose}}$ of 1.220 the $\Delta n_{\text{protein}}$ goes back to the expected level based on linear drift of $\Delta n_{\text{protein}}$. This slightly different $R_{660/457}^{\text{glucose}}$ remains within the error margins of the individually measured ratio for D-glucose, such that the difference can be explained by differences in response of the sensor per measurement. Amplitudes of $\Delta n_{\text{glucose}}$ should not be compared with $\Delta n_{\text{protein}}$ as scaling is required.

4.2.2 Beads and D-glucose

In a similar way as for the protein A and D-glucose, Fig. 1(d) was analysed with the theoretical model as shown in Fig. 1(e). The optimal result was realized based on a d_{core} of 63.4 nm and d_1 of 70 nm, which is lower than the expected 85 ± 6.5 nm. This might partly be explained by the fact that the beads are spherical and not cubical, as the response of the ΔN_{eff}'s induced by a cubic shaped particle binding on the sensor surface is similar to the response of the ΔN_{eff}'s induced by a larger spherical shaped bead binding on the same sensor surface. By subtracting the Δn_{l_2} from Δn_{l_1} and assuming low concentrations and bulk changes occurring in both layers it was again possible to determine a signal which should belong to only the beads. The determined $\Delta n_{l_2} - \Delta n_{l_1}$ is equal to approximately $1.6\text{x}10^{-3}$ RIU, which corresponds to a surface fractional coverage of the beads of approximately 0.2%.

Using the ratio-based approach, $\Delta n_{\text{glucose}}$ and Δn_{bead} were determined, again based on the measured ratios of the individual substances. As expected, the Δn_{bead} does not increase when adding D-glucose, increases when adding the beads and remains constant after applying a washing step. The $\Delta n_{\text{glucose}}$ reaches a level which is approximately the same as in Fig. 1(c) as expected because the added D-glucose concentrations were the same. However, after the washing step the $\Delta n_{\text{glucose}}$ is a bit lower than expected. An optimal result is given at $R_{660/457}^{\text{bead}}$ = 0.900 which again remains within measured error bars of $R_{660/457}^{\text{bead}}$.

#257853 Received 5 Feb 2016; revised 14 Mar 2016; accepted 15 Mar 2016; published 12 Apr 2016

4.2.3 Protein A and beads

For the measurement of simultaneous addition of beads and protein A the approach based on theoretical analysis is not very suitable, especially because Δn_{l_2} is far from homogeneous as the evanescent field penetrates deeper than the thickness of the bead. Moreover, the expected end levels of the protein A and the beads are not known which was known for the bulk effect of the D-glucose. Consequently, the fitting of d_1 is not feasible.

Using the ratio-based approach it is possible to discriminate between the protein A and the beads. The result based on ratios of ratios measured for the individual substances is shown in Fig. 1(i). As was mentioned, amplitudes between $\Delta n_{\text{protein}}$ and Δn_{bead} should not be compared as scaling factors of substances are individual. However, $\Delta n_{\text{protein}}$ of Fig. 1(i) can be compared with $\Delta n_{\text{protein}}$ of Fig. 1(c). In Fig. 1(i) half of protein A was added to the sensor, but the measured $\Delta n_{\text{protein}}$ is only 1.6 times lower. An even lower signal of $\Delta n_{\text{protein}}$ is expected as now also beads can cover part of the surface where beads can bind. Furthermore, the Δn_{bead} of Fig. 1(f) is approximately 2.6 times higher compared to Δn_{bead} of Fig. 1(i), where the added beads concentration was two times lower. The differences might be explained that different chips and different stock solutions were used for the different measurements. Furthermore, all the measurements are based on the non-specific adhesion of the protein A and the beads to the sensor surface. Therefore, small differences between sensor surfaces can make a large difference. The result from D-glucose in which no binding is involved, the signals were in nice agreement with each other. Determined RI changes due to non-specific binding of particles and between different measurements should not be compared if not all the conditions (chip, stock solution, analysis parameters) of the measurements are the same.

Besides, Fig. 1(i) shows that using two ratios, excluding $R_{660/457}^{\text{glucose}}$, it is not possible to suppress the first D-glucose step from the protein and beads signal. Three wavelengths are required to discriminate between protein A, 85 nm beads and D-glucose in a single measurement, as presented in the Appendix C.

4.3 Blind experiment

To approve the usability and verify the correctness of the ratio-based approach a blind experiment was carried out. Six combined samples of protein A (in the range of 0.1 - 1.0 μg/ml) and 85 nm beads (in the range of 0.4 - 4.0 μg/ml) were made and labelled by an independent person. Before measuring, the samples were carefully mixed to ensure homogeneous solutions. Next, the samples were measured in two measurement sets performed on the same waveguide using three measurement channels and one reference channel. In between the measurement sets the waveguides were cleaned using a cleaning protocol with can be found in Appendix G. A D-glucose characterization step was applied to verify the correct response at the different wavelengths. This resulted in a different ratio of the measured ΔN_{eff}'s of 1.263 compared to the 1.218 ± 0.016. This can be explained by the fact that we used a different chip for this measurement which can have for example a slightly different d_{core}. To correct for this deviation, we changed the average measured ratios of the individual substances by multiplying them by $1.263/1.218$ and used this for the ratio-based approach to analyse this experiment. Figure 2(a) shows an example of a measurement with the D-glucose characterization step and adding sample A and Fib. 4b shows the corresponding determined Δn_{bead} and $\Delta n_{\text{protein}}$ over time, which are read out at t = 2400 s when the beads signal was constant. The expected values of Δn based on linear drift (baseline determined between t = 1320 s and t = 1380 s) are subtracted from this $n_{t=2400s}$ and plotted as a function

#257853 Received 5 Feb 2016; revised 14 Mar 2016; accepted 15 Mar 2016; published 12 Apr 2016

of the applied concentration in Fig. 2(c) and Fig. 2(d) for the 85 nm beads and the protein A respectively.

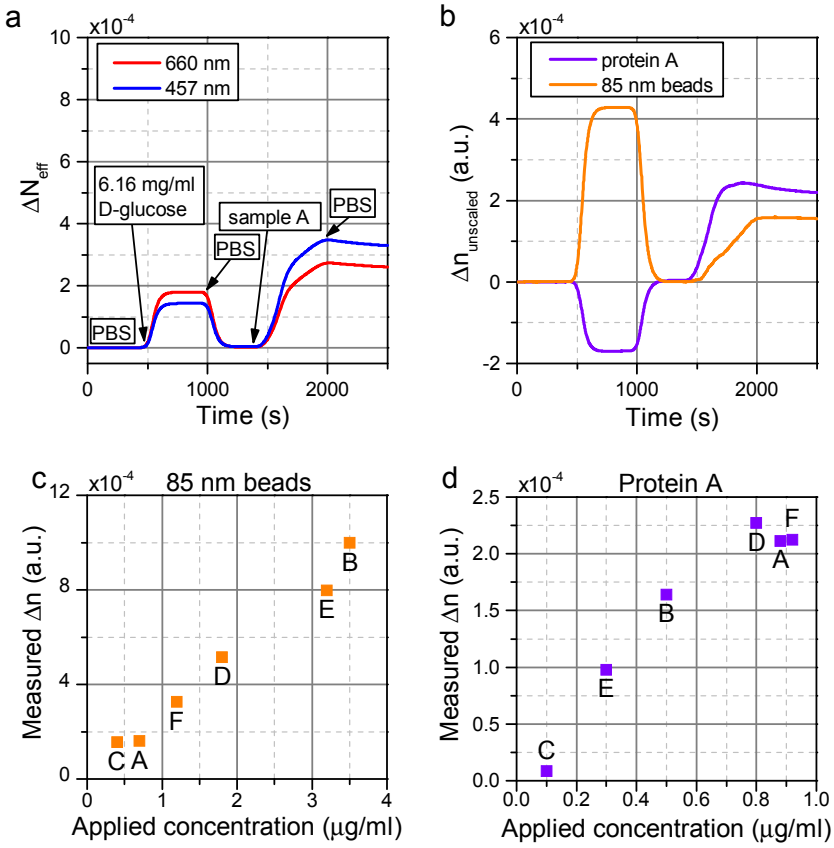

Fig. 2. Blind experiment with six samples (A-F) containing 85 nm beads and protein A. a) The measured ΔN_{eff} over time of one measurement of the set of blind experiments b) the corresponding determined Δn_{beads} and $\Delta n_{protein}$ using the ratio-based approach and c) the determined Δn as a function of the by forehand unknown applied concentrations of the 85 nm beads and d) the determined Δn as a function of the by forehand unknown applied concentrations of the protein A. For visibility reasons, the data points A and F of the applied protein concentration are slightly offset but they both correspond to 0.9 µg/ml.

The applied bead concentration and the determined Δn_{bead} show a linear trend which means the Δn_{bead} was determined correctly using the ratio-based approach, assuming a linear relation between the number of beads in the sample and response of the sensor. Moreover, it shows that it is possible to do a calibration experiment to find the relations between the beads concentration and the response of the sensor. Furthermore, also a linear trend is seen between the measured $\Delta n_{\text{protein}}$ and the applied protein concentration. Only at higher applied protein A concentrations, the determined $\Delta n_{\text{protein}}$ flattens off, which can be explained by the fact that for these measurements the surface was saturated with protein A which can be seen in Fig. 2(b). That the signal of Δn_{bead} still increases might be explained by the beads replacing the protein A of the surface. The be able to compare Δn_{bead} and $\Delta n_{\text{protein}}$, the signals were both read out at the same time point. The blind experiment illustrates that the determined $\Delta n_{\text{substance}}$

#257853 Received 5 Feb 2016; revised 14 Mar 2016; accepted 15 Mar 2016; published 12 Apr 2016

can be compared with the $\Delta n_{\text{substance}}$ of a different experiment, when using the same measurement conditions (chip, stock solution, analysis parameters).

4.4 Noise, drift and artefacts in measurements

Here, we shortly discuss the influence noise, drift and artefacts in $\overline{\Delta N_{eff}}$ on $\overline{\Delta n}$. All noise sources in the signal of $\overline{\Delta N_{eff}}$ are enhanced using the above named approaches, which means that they are stronger visible in $\overline{\Delta n}$. This can be explained by the matrix becoming more singular, resulting in enhancement of all kind of noise sources. Linear drift measured in ΔN_{eff}'s (e.g. due to temperature changes causing relative movement between chip and CCD camera or causing directly a Δn at the sensing windows) results in linear drift in Δn of both layers (see Appendix E). For the measurements we assume linear drift and take this into account when fitting $R^{s_m}_{\lambda_k/\lambda_l}$ or waveguide parameters. Moreover, artefacts (fluctuations e.g. seen in Fig. 1(f) at $t \approx 500$ s and 1000 s in $\Delta n_{\text{protein}}$, but better visible at discrimination between three substances using three wavelengths, see Appendix C) show up in $\overline{\Delta n}$. These artefacts are present in the signal of the ΔN_{eff}'s, but are not visible because of the relatively higher slopes of ΔN_{eff} due to the fast addition of the sample. The artefacts are caused by boundary effects of the shifting interference pattern (see Appendix D). When inducing a linear $\Delta\varphi$ in the interference pattern this results in a oscillation in the amplitude of the spatial frequency as it is not constant when the fringes move. It also results in a oscillation in $\Delta\varphi$ which is directly related to $\overline{\Delta N_{eff}}$. Using a proper windowing function (e.g. Blackman-Nuttall) we were able to remove the oscillations from simulated shifting interference patterns. However, this was not sufficient for the measured data, possibly because of non-ideal properties of the lenses, the grating and beam shape (see Appendix D). Therefore, the artefacts in $\overline{\Delta N_{eff}}$ can result in misfits of the fitted $R^{s_m}_{\lambda_k/\lambda_l}$ or waveguide parameters. The spread in the determined d_{core}, d_{layer} and $R^{s_m}_{\lambda_k/\lambda_l}$ can be caused by especially the artefacts, resulting in a wrongly determined $\overline{\Delta n}$. The signal of $\overline{\Delta n}$ becomes especially very noisy in the case when discriminating between three Δn 's based on three ΔN_{eff} 's (see Appendix C). To be able to use this method for three wavelengths to solve three independent Δn's, the artefacts in the measurement should be reduced by for example testing if larger optical components reduce the artefacts.

5. Summary and conclusions

By measuring the ΔN_{eff} at two different wavelengths it was possible to discriminate between two different substances inducing a Δn in the evanescent field of the sensor. The binding of 85 nm beads or protein A was discriminated from D-glucose and the binding of 85 nm beads was discriminated from the binding of protein A. Using three ΔN_{eff}'s to discriminate between three different substances inducing a Δn, the result became more noisy. For a successful application of these analysis approaches used to determine three independent Δn's, the artefacts (due to boundary effects of the shifting interference pattern, see Appendix D) in ΔN_{eff} should be reduced significantly. Alternatively, other techniques to improve specificity can be used next to size-selective detection. For example, to discriminate the binding of beads from binding of protein A and bulk changes due to D-glucose, D-glucose can also be added to

#257853 Received 5 Feb 2016; revised 14 Mar 2016; accepted 15 Mar 2016; published 12 Apr 2016

the reference channel to cancel out the contribution due to D-glucose. In that case only two wavelengths are required to discriminate between binding of beads and proteins, resulting in less enhancement of noise.

Application of a approach based on theoretical analysis made it possible to discriminate between Δn's occurring in different layers in the evanescent field, assuming a homogeneous Δn in each layer. However, to determine the correct value for Δn, this method requires multiple parameters (e.g. the waveguide core thickness, waveguide RIs, layer thicknesses, wavelengths) to be tuned that is difficult and labour-intensive. Therefore, also a much more pragmatic ratio-based analysis approach is presented to discriminate between Δn's induced by different substances. Moreover, this approach can be used for different substances inducing a Δn in overlapping layers, which is not always possible with the approach based on theoretical analysis. Information on the absolute amplitude of Δn_s is lost using the ratio-based approach, however for determining an analyte concentration calibration measurements can be performed which are usually also required using an YI with a single wavelength. 85 nm beads, D-glucose and protein A were discriminated from each other using this ratio-based approach. The working of the ratio-based approach was verified by a blind experiment with different samples containing different concentrations of protein A and beads. We could discriminated Δn_{bead} from $\Delta n_{\text{protein}}$, resulting in an expected linear trend of the Δn_{bead} with the applied concentration. So here we discriminate between protein A (≈2 nm large) and 85 nm beads, but this can raise the question what would be the minimal size difference of discriminable substances. It is very difficult to say something general about this as the minimal discriminable size difference depends on a number of parameters such as the amplitude of the signals of the substances and the amplitude of the noise, artefacts and drift of the phase signal. When a certain application is identified, then the sensor should be optimized to determine the limits of the device for the specific application in mind. Size-selective analyte detection can for example be used to discriminate specific analyte binding of larger particles from non-specific binding of smaller particles. Therefore, we believe that with measuring size-selectivity we can strongly improve the performance of our YI sensor and IO interferometric sensors in general. Especially the ratio-based approach is an easy approach to discriminate between different substances causing a Δn.

Appendix A: Experimental details

In this section we describe the experimental details of the setup which was used for the measurements presented in the main text and in the rest of the appendices.

A.1 Sample transportation

Samples are degassed by a 4-channel Degassi Classic degasser and transported to the sensor surface by a 4-channel Ismatec® Reglo Digital Peristaltic Pump with a flow rate of 100 µl/min towards the sensing windows of the waveguide structure. On top of these sensing windows a 100 µm high fluid cuvette is placed to transport the sample to the sensor with a laminar flow, which means that in the evanescent field that is used for detection the velocity is nearly zero and transport of the different substances is determined by diffusion.

A.2 Hardware

Measurements are performed in a 4-channel single-mode ridge waveguide YI sensor. The waveguide consists three layers: a PECVD SiO_2 layer covering a LPCVD Si_3N_4 70 nm thick core on top of a thermal SiO_2 substrate. A sensing window with a length l of 4 mm is created by etching away the PECVD SiO_2 cover. Measurements are done with one single waveguide structure (chip) which is cleaned after each measurement (see Appendix G). The wavelengths 457, 561 (only used when discriminating between three substances) and 660 nm are chosen such that only zero order TE modes (in height) fit into the waveguide and such that

#257853 Received 5 Feb 2016; revised 14 Mar 2016; accepted 15 Mar 2016; published 12 Apr 2016

wavelengths are well spread, which is required to achieve a good precision [15]. The different light sources are coupled into a single mode polarization maintaining (SMPM) fiber which can be positioned with respect to the waveguide using an *xyz*-stage to be able to quickly and sufficiently couple all wavelengths into the waveguide. The fiber tip is strengthened with a glass ferule which is positioned against the waveguide with a matching index gel in between them to prevent reflections at the interfaces which resulted in a oscillations of the phase signal. Figure 3 shows a schematic overview of the hardware of the setup.

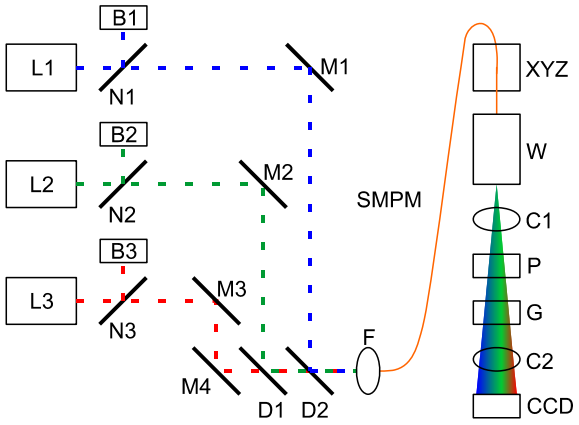

Fig. 3. Setup. Schematic overview of the setup where L1-L3 are a 50 mW Cobolt Twist 457 nm Single Longitudinal Mode (SLM) Diode-Pumped Solid State (DPSS) laser, a 50 mW Cobolt Jive 561 nm SLM DPSS laser and a 50 mW Cobolt Flamenco 660 nm SLM DPPS laser respectively of which the power is regulated using Thorlabs NDC-100C-4M mounted variable ND filters (N1-N3) of which the reflected light is directed to Thorlabs BT500 beam dumps. Next, Thorlabs, BB1-E02 visible broadband dielectric mirrors (M1-M4) and a Semrock Di01-R561-25x36 dichroic mirror (D1) and a Semrock Di01-R442-25x36 dichroic mirror (D2) are used to overlap the three lasers which are subsequently coupled into a Thorlabs PM460-HP single mode polarization maintaining (SMPM) fiber using a Schäfter + Kirchhoff GmbH 60FC-4-RGBV11-47 apochromatic fiber collimator (F). This fiber is positioned on a ULTRAlign Precision XYZ Positioning Stage (XYZ) with DS-4F High Precision Adjusters to position the fiber with respect to the YI waveguide (W) in order to efficiently couple the light via butt-end coupling into this 4-channel single-mode ridge waveguide. After the light is coupled out of the waveguide it will form an interference pattern which is collimated in the horizontal plane using a Thorlabs, ACY254-075-A cylindrical achromatic lens (C1). Subsequently, the interference pattern passes a Thorlabs LPVISE100-A linear polarizer with 400-700 nm N-BK7 protective windows (P) to filter out possible converted TM polarized light. Next, the light is directed to a Thorlabs, GT-25-03 25mm x 25mm 300 lines/mm visible transmission grating (G) to separate the different wavelengths after which it passes a Thorlabs ACY254-050-A cylindrical achromatic lens (C2) which images the interference patterns on a Alta U30-OE CCD camera (CCD).

A.3 Analysis

A Fast Fourier Transform (FFT) is applied to the interference patterns detected with the CCD camera. Different windows were applied to the interference patterns to prevent boundary effects (see Appendix D). Subsequently, spatial frequency peaks of the interference pattern are determined such that the phase change $\Delta\varphi$ ($\propto \Delta N_{eff}$) of each channels pair can be read out. For the measurements we only use one channel pair combination (one measurement channel and one reference channel) and the rest is neglected, expect for the blind experiment for which we use all channels.

#257853 Received 5 Feb 2016; revised 14 Mar 2016; accepted 15 Mar 2016; published 12 Apr 2016

Appendix B. Ratio-based analysis approach

B.1 Effective refractive index ratios at various wavelengths

The ratios $R^{s_m}_{\lambda_n/\lambda_m}$ are experimentally determined for three different wavelengths (λ_1=457 nm, λ_2=561 nm and λ_3=660 nm), and for three different substances: 85 nm carboxylated polystyrene beads, protein A and D-glucose (see Table 1), representing specific binding, non-specific binding and bulk changes respectively. Figure 4 shows an example of a measurement with D-glucose and 85 nm beads measured at λ_1=457 nm and λ_3=660 nm, illustrating the difference in $R_{660/457}$ for both substances. A single value for the ratio for a given substance is determined by calculating the mean value of the ratios over the time interval in which the ratios have a relatively stable value for that substance. In practice it was found that the time intervals that show a stable ratio correspond to intervals in which N_{eff,λ_1} was between 80 - 100% of its maximum value for D-glucose, 20 - 100% for 85 nm beads and 10 - 100% for protein A. Therefore these intervals were applied for determination of all ratios.

Figure 5 shows all determined values of $R^{s_m}_{\lambda_n/\lambda_m}$ and their mean and corresponding 95% confidence interval (error bars, twice the standard deviation). The ratios $R^{s_m}_{\lambda_n/\lambda_m}$ and corresponding confidence intervals are also listed in Table 1.

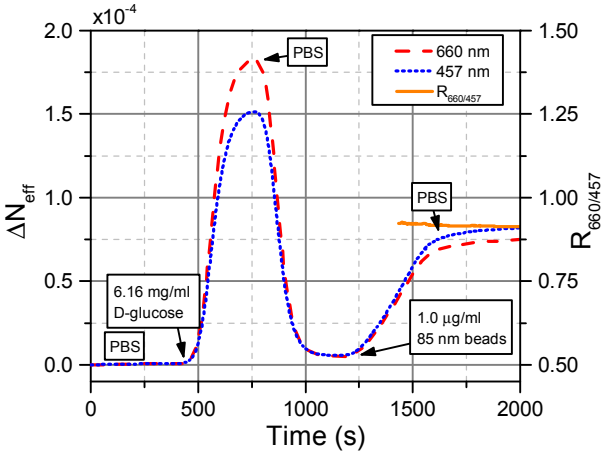

Fig. 4. The ΔN_{eff} measured at 457 nm (blue line) and at 660 nm (red line) when adding 6.16 mg/ml D-glucose and 1.0 µg/ml 85 nm carboxylated polystyrene beads to the sensor plotted on the left axis and the corresponding ratio $R_{660/457}$ (orange line) plotted on the right axis.

#257853 Received 5 Feb 2016; revised 14 Mar 2016; accepted 15 Mar 2016; published 12 Apr 2016

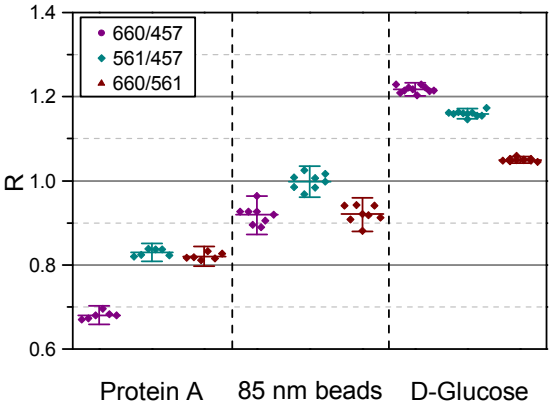

Fig. 5. Measured ratios $R^{s}_{\lambda_n/\lambda_m}$ (dots, diamonds and triangles) for protein A, 85 nm carboxylated polystyrene beads and D-glucose for all combinations of the wavelengths 457 nm, 561 nm and 660 nm. Also indicated is the average of the measured ratios and the corresponding error bars representing the 95% confidence interval.

Table 1. Measured effective refractive index ratios. Experimentally determined ΔN_{eff} ratios at λ_1 = 457 nm, λ_2 = 561 nm and λ_3 = 660 nm determined for D-glucose, 85 nm carboxylated polystyrene beads and protein A.

	$R_{660/457}$	$R_{561/457}$	$R_{660/561}$
D-glucose	1.218 ± 0.016	1.160 ± 0.012	1.050 ± 0.008
85 nm beads	0.918 ± 0.045	0.998 ± 0.037	0.920 ± 0.040
Protein A	0.680 ± 0.022	0.830 ± 0.022	0.820 ± 0.023

B.2 Theory of ratio-based analysis method

Here, we derive Eq. (3) of the manuscript. When a substance s_m is added to the sensor it induces a Δn_{s_m}, this results in an effective refractive index change $\Delta N_{eff,\lambda_k}$ at λ_k. Assuming that the response of the sensor has a linear relationship with the amount of s_m that is added to the sensor, this can be written as:

$$\Delta N_{eff,\lambda_k} = \frac{\partial N_{eff,\lambda_k}}{\partial n_{s_m}} \Delta n_{s_m}, \tag{4}$$

where $\partial N_{eff,\lambda_k} / \partial n_{s_m}$ is the sensitivity coefficient of the sensor for a RI change induced by s_m. Assuming that substances do not influence each other's response of the sensor, multiple substances inducing different ratios can be discriminated from each other using:

$$\overline{\Delta N_{eff}} = \overline{\overline{S_{sub}}} \cdot \overline{\Delta n_s}, \tag{5}$$

where the vector $\overline{\Delta N_{eff}}$ is composed of the elements $\Delta N_{eff,\lambda_k}$, the vector $\overline{\Delta n_s}$ is composed of the elements Δn_{s_m}, and the coefficients of matrix $\overline{\overline{S_{sub}}}$ are given by $s_{k,m} = \partial N_{eff,\lambda_k} / \partial n_{s_m}$.

Next, we define the ratio of two ΔN_{eff}'s measured at two wavelengths λ_k and λ_l, induced by a substance s_m as:

#257853 Received 5 Feb 2016; revised 14 Mar 2016; accepted 15 Mar 2016; published 12 Apr 2016

$$R_{\lambda_k/\lambda_l}^{s_m} = \frac{\Delta N_{eff,\lambda_k}^{s_m}}{\Delta N_{eff,\lambda_l}^{s_m}} = \frac{\partial N_{eff,\lambda_k}^{s_m} \big/ \partial n_{s_m} \cdot \Delta n_{s_m}}{\partial N_{eff,\lambda_l}^{s_m} \big/ \partial n_{s_m} \cdot \Delta n_{s_m}} = \frac{s_{k,m}}{s_{l,m}}. \tag{6}$$

where we neglect the dispersion in Δn_{s_m}. We can express the elements of matrix $\overline{\overline{S_{sub}}}$ in terms of the ratios $R_{\lambda_k/\lambda_l}^{s_m}$. Due to the fact that $R_{\lambda_k/\lambda_l}^{s_m} = 1 \big/ R_{\lambda_l/\lambda_k}^{s_m}$ and $R_{\lambda_k/\lambda_l}^{s_m} = R_{\lambda_k/\lambda_j}^{s_m} \big/ R_{\lambda_l/\lambda_j}^{s_m}$ we can rewrite Eq. (5) as:

$$\overline{\Delta N_{eff}} = \overline{\overline{R}} \cdot \overline{\overline{\Theta}} \cdot \overline{\Delta n_s}, \tag{7}$$

where $\overline{\overline{\Theta}}$ is a matrix with theoretical sensitivity coefficients of which the elements are given by $\theta_{k,m} = S_{\lambda_k, s_m} \forall\, k = m$ and $\theta_{k,m} = 0 \forall\, k \neq m$, and the coefficients of matrix $\overline{\overline{R}}$ are given by $r_{k,m} = R_{\lambda_k/\lambda_m}^{s_m}$. To determine $\overline{\Delta n_s}$ Eq. (7) can be rewritten as:

$$\overline{\Delta n_s} = \overline{\overline{\Theta}}^{-1} \cdot \overline{\overline{R}}^{-1} \cdot \overline{\Delta N_{eff}}. \tag{8}$$

Appendix C. Discrimination between three different-sized substances

To test if both analysis approaches are also applicable when using three wavelengths to discriminate three Δn's induced by three different substances, D-glucose (6.16 mg/ml), 85 nm carboxylated polystyrene beads and protein A were added to the sensor after each other. The ΔN_{eff} was measured at λ_1=457 nm, λ_2=561 nm and λ_3=660 nm as shown in Fig. 6(a). Figure 6(b) shows the Δn corresponding to Fig 6(a) determined with the approach based on theoretical analysis after fitting the d_{core}, d_1 and d_2 based on analysing the results based on two wavelengths. An example of this is shown in Fig. 6(c) where d_{core} and d_2 were determined as 62.7 nm and 64 nm respectively, based on λ_1 and λ_3. It can be seen that at the D-glucose step the Δn_{l_1} and Δn_{l_2} are equal and when adding the beads at t_3 there is an increase of Δn_{l_1} and Δn_{l_2} stays approximately constant. Similarly, the fitting was done with λ_1 and λ_2, and for the combination of D-glucose and protein A and the combination of protein A and beads, based on the wavelength combination λ_1 with λ_2 and λ_1 with λ_3. This resulted in a d_{core} = 62.55 ± 0.15 nm, d_1 = 5 ± 2 nm and d_2 = 60 ± 4 nm, illustrating that combinations of ΔN_{eff}'s measured at different wavelengths give different fit values, indicating that the parameters in the theoretical model are probably not completely right and that artefacts (see Appendix D) play a significant role here. The result in Fig. 6(b) is based on the average values for d_{core}, d_1 and d_2 and three wavelengths to discriminate between the three layers. The overall signals determined with the approach based on theoretical analysis based on three wavelengths/layers is much more noisy compared to the two wavelengths/layers case, which makes the optimization more difficult. The increase in noise, artefacts and drift can be explained by the fact the matrix to $\overline{\Delta n_l}$ from $\overline{\Delta N_{eff}}$ becomes more singular and therefore all noise sources are enhanced which was already shown by [15]. However, ignoring the noise, drift and artefacts, all signals increase roughly with the same amplitude when adding D-glucose at t_1 (Δn_{l_1} has a much higher amplitude, so is plotted on a different scale). When adding the beads, an increase in Δn_{l_1} and Δn_{l_2} is expected, but there is also an increase of Δn_{l_3}. Also when adding protein A at t_5 there is an unexpected decrease of Δn_{l_2} and unexpected increase of Δn_{l_3} as it was only expected that Δn_{l_1} would increase. These things probably mean that the signals Δn_{l_1}, Δn_{l_2}

#257853 Received 5 Feb 2016; revised 14 Mar 2016; accepted 15 Mar 2016; published 12 Apr 2016

and Δn_{l_3} are not sufficiently decoupled. Optimizing the theoretical matrix further is more complex compared to the two wavelengths/layers situation, because changing one parameter will result in change of all the signals Δn_{l_1}, Δn_{l_2} and Δn_{l_3}, illustrating the complexity and limits of the approach based on theoretical analysis. Therefore, we ratio-based approach is better used for this analysis.

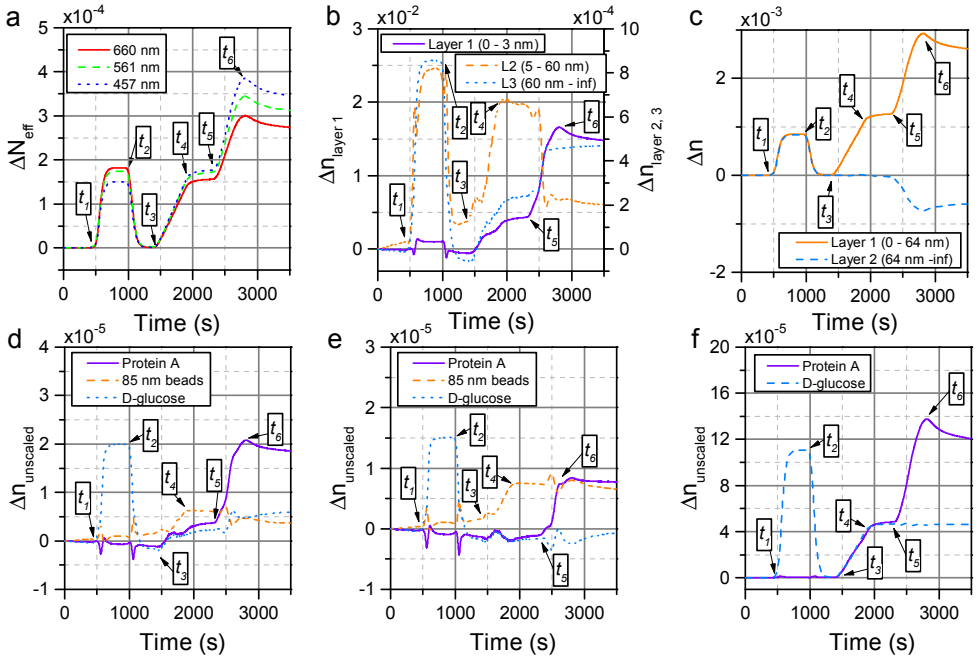

Fig. 6. Three substances discriminated from each other. a) The ΔN_{eff} measured over time starting with a PBS buffer, adding 6.16 mg/ml D-glucose at t_1 resulting in higher ΔN_{eff} for the longer wavelengths as expected. After applying a washing step at t_2, 1.0 µg/ml 85 nm beads was added at t_3. The response of the shorter wavelengths is now larger. After washing again with PBS at t_4, 2.0 µg/ml protein A was added at t_5 resulting in a relatively stronger response of the shorter wavelengths. After applying a washing step at t_6 the signal decreases due to desorption of the protein A, b) the corresponding $\overline{\Delta n_{layer}}$ determined with the approach based on theoretical analysis fitting d_{core}, d_1 and d_2 based on analysing the measurement with two wavelengths (see example shown in c)), the $\overline{\Delta n_{\text{substance}}}$ determined with ratio-based approach based on d) the ratios measured with the individual substances and e) after tuning the ratios based on analysing the measurement with two wavelengths and two substances of which an example is given in f).

Figure 6(d) shows the determined $\overline{\Delta n_s}$ with the ratio-based approach. The ratios used for the analysis are again based on the determined ratios of ΔN_{eff} at the different wavelengths for the individual substances. Between t_1 and t_2 only $\Delta n_{\text{glucose}}$ changes apart from some fluctuations seen for Δn_{bead} and $\Delta n_{\text{protein}}$, which can be explained by boundary effects of the shifting interference pattern (see *section 4.4 Noise, drift and artefacts in measurements* in main text). At t_3 the beads where added, but besides the increase of Δn_{bead} there is also an increase of $\Delta n_{\text{protein}}$ and $\Delta n_{\text{glucose}}$ which means that the signals of $\overline{\Delta n_s}$ are not perfectly decoupled. This is also the case at t_5 when protein A is added to the sensor which mainly

#257853 Received 5 Feb 2016; revised 14 Mar 2016; accepted 15 Mar 2016; published 12 Apr 2016

result in an increase of $\Delta n_{\text{protein}}$, but also in a small increase of $\Delta n_{\text{glucose}}$. Therefore, the ratios were also optimized by analysing the measurement based on two wavelengths/substances. An example is shown in Fig. 6(f), which shows that $\Delta n_{\text{protein}}$ was sufficiently decoupled from $\Delta n_{\text{glucose}}$ based on λ_1 and λ_3. Because only two wavelengths were used to discriminate between $\Delta n_{\text{protein}}$ and $\Delta n_{\text{glucose}}$ it was not possible to discriminate them from Δn_{bead} which is shown between t_3 and t_4 where both $\Delta n_{\text{protein}}$ and $\Delta n_{\text{glucose}}$ increase. Figure 6(e) shows the result of $\overline{\Delta n_s}$ after optimization of the ratios which led to $R_{561/457}^{\text{protein}}$=0.837, $R_{660/457}^{\text{protein}}$=0.698, $R_{561/457}^{\text{bead}}$=0.967, $R_{660/457}^{\text{bead}}$=0.885, $R_{561/457}^{\text{glucose}}$=1.158 and $R_{660/457}^{\text{glucose}}$=1.215 from which $R_{660/561}^{s_m}$ can be calculated by dividing $R_{660/457}^{s_m}$ by $R_{561/457}^{s_m}$. All these values fall within the error margins of the experimentally determined ratios of the individual substances presented in Table 1. Using the slightly changed ratios, the three substances are nicely decoupled, illustrating that it is possible to discriminate between three different substances. However, the enhanced drift and artefacts in $\overline{\Delta n_s}$ makes it difficult to analyse these results. Moreover, when substances were added simultaneously (data not shown here) fitting based on two substances/two wavelengths is not possible. Therefore, the ratios used for the analysis should be measurable from measurements with the single substances and not be tuned afterwards. To realise this the spread in ratios should be reduced. More research is required to determine what the origin of the spread of the ratios is. In order to do this, it should be investigated if the spread can be explained by the artefacts or other noise sources of the measurements, the cleaning of the surfaces of the chip (larger spread is seen in binding of substances compared to bulk changes due to D-glucose) or the substances self (spread in protein A is smaller compared to beads). At least it is required to reduce the aforementioned artefacts which are enhanced too much when using three wavelengths to discriminate between three substances.

Appendix D. Artefacts in signal due to boundary effects of shifting interference pattern

Computer generated images of interference patterns (based on our four channel Young interferometer) were used to verify the correct working of the Labview program which is used to collect interference patterns and determine the corresponding phase changes during an experiment, to investigate artefacts when determining a phase change from a finite interference pattern and to test windowing functions to reduce artefacts. Calculations of the generated interference patterns are based on four point sources distanced at 60 µm, 80 µm and 100 µm, an imaged distance of 17.5 cm, and wavelengths of 457 nm and 660 nm. The generated images have a width of 1024 pixels, a height of 100 pixels and a dynamic range of 60000 counts and include shot noise (Poisson noise). To simulate a real experiment, a time varying ΔN_{eff} ($\sim\Delta\varphi$) is introduced (see Fig. 7(a)). For each corresponding time point an image is calculated and stored for later analysis. Next, the Labview program loads the images, adds up the selected number of rows on which the interference patterns are imaged and subsequently adds 1024 zeros to increase spatial frequency resolution to improve phase readout. Optionally, a windowing function is applied before a Fast Fourier Transform (FFT) is executed. From the resulting spectrum, the phase and amplitude of the six different spatial frequencies are determined of which we now analyse one peak belonging to one channel pair. Figure 7(a) shows an example of the induced and calculated ΔN_{eff} for the two wavelengths. The same figure also shows the difference in ΔN_{eff} between the induced and determined values. Figure 7(b) shows the determined amplitude and Fig. 7(c) shows the $\overline{\Delta n_{\text{substance}}}$ determined with the ratio-based approach based on the induced (ind) and determined (det) $\overline{\Delta N_{eff}}$. Figure 7(d), 7(e) and 7(f) show the $\overline{\Delta N_{eff}}$, the amplitude and the determined

#257853 Received 5 Feb 2016; revised 14 Mar 2016; accepted 15 Mar 2016; published 12 Apr 2016

$\overline{\Delta n_{\text{substance}}}$ of a real measurement. Similar fluctuations (which we call artefacts) are seen in in the amplitude and $\overline{\Delta n_{\text{substance}}}$ when no windowing is applied on the simulated interference patterns. These artefacts are most prominent during (fast) changes in the induced ΔN_{eff}.

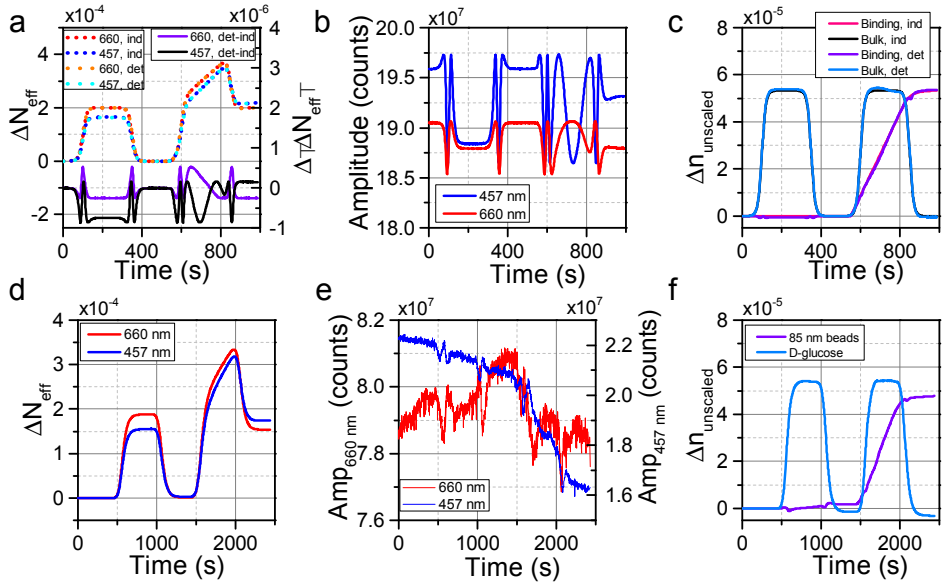

Fig. 7. Comparison of fluctuations in the ΔN_{eff} as determined by using simulated data (a,b,c) and measured data (d,e,f) in a typical measurement composed of a bulk signal followed by a combination of a bulk signal and a signal arising from surface binding. a) ΔN_{eff} induced (ind) and determined by analysing simulated data without applying a window (det) and the difference between detected and induced ΔN_{eff}, b) the amplitude determined by the FFT corresponding to the $\Delta\varphi$ from which ΔN_{eff} is determined, c) Δn as induced and as determined using the ratio-based approach, d) the ΔN_{eff} of a measurement where first D-glucose was added, followed by adding simultaneously D-glucose and 85 nm beads to the sensor surface, e) the corresponding amplitude of the FFT-spectrum at the measured spatial frequency and f) the determined Δn due to binding of the beads and bulk changes due to the D-glucose.

To investigate this further, a linear $\Delta\varphi$ ($\sim\Delta N_{eff}$) was induced and the peak-to-peak (pk-pk) values of the artefacts in ΔN_{eff} were determined to test the influence of the applied window on the size of the artefacts (both in amplitude and $\Delta\varphi$ ($\sim\Delta N_{eff}$)). Figure 8(a) shows the linear ΔN_{eff} determined from the linear $\Delta\varphi$, and the difference between the determined and induced ΔN_{eff} ($=\Delta N_{eff}$ error, abbreviated as NE in the remainder of the text) for the case in which no window is applied and the case in which a in Labview build-in Blackman-Nuttall window is applied. Figure 8(b) shows the mean pk-pk values of the NE of different channel combinations, determined from $\Delta\varphi$ measured at the spatial frequencies (sf) belonging to the channel combination in which a Δn was generated in one of the channels as well as from the channel combinations in which no Δn occurred (cross-talk, CT). To demonstrate the effect of windowing, results are plotted for different type of windows. For example, applying a Blackman-Nuttall or a Dolph-Chebyshev window, both CT and NE can be completely

#257853 Received 5 Feb 2016; revised 14 Mar 2016; accepted 15 Mar 2016; published 12 Apr 2016

suppressed down to the shot-noise level as the artefacts were not visible above the shot-noise level.

Next, the use of different windows on real experimental data is evaluated. The mean pk-pk values of CT are similar to the mean pk-pk values of NE. Therefore, the mean pk-pk values of CT are used as a measure for the pk-pk values of NE for the real experiments, as it is not possible to determine the fluctuations in the measured signal of ΔN_{eff}, because the slope of

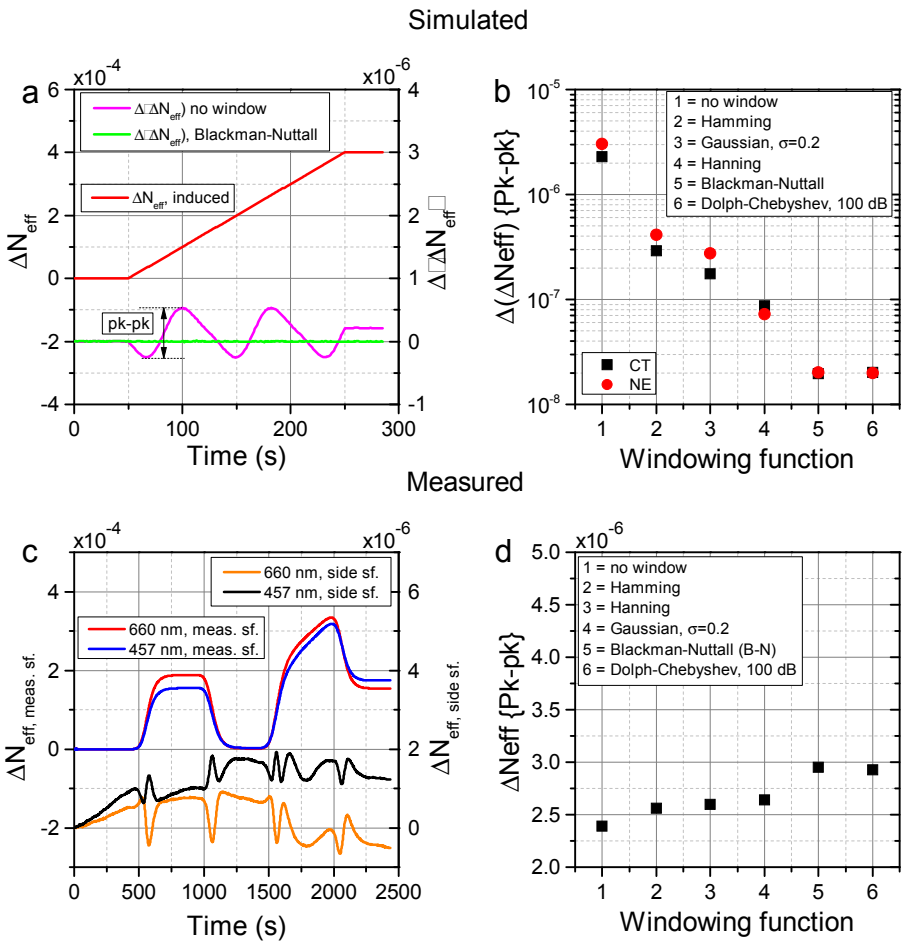

Fig. 8. The effect of applying different windows on the data on the error in the determined phase change ($\sim \Delta N_{eff}$). a) ΔN_{eff} induced and the difference between determined and induced ΔN_{eff} (NE) applying no window (magenta) and a Blackman-Nuttall window (green), b) the peak-to-peak (pk-pk) values of the fluctuations in ΔN_{eff} (for both NE and CT) for the different applied window, c) the measured ΔN_{eff} of a measurement channel and the CT in a side channel and d) the pk-pk values of the fluctuations in ΔN_{eff} due to CT as a function of the applied windowing function of the interference pattern.

the measured signal is much higher than the slope of the artefacts. Also no induced ΔN_{eff} can be determined and consequently it is not feasible to determine the difference between a measured and induced ΔN_{eff} to determine the NE. Raw data (interference patterns) were

#257853 Received 5 Feb 2016; revised 14 Mar 2016; accepted 15 Mar 2016; published 12 Apr 2016

saved and different windows were applied on the measured data. Figure 8(c) shows the fluctuations in ΔN_{eff} due to CT for a typical measurement where first D-glucose only (between $t \approx 500$ and 1000 s) and subsequently D-glucose plus 85 nm beads (between $t \approx 1500$ and 2000 s) were added simultaneously to the sensor. Figure 8(d) shows the pk-pk value of the first artefact in ΔN_{eff} (at $t \approx 500$ - 700 s) due to CT as a function of the applied window. Applying different windows did not lead to significant differences in performance. Probably the measured interference patterns already contains a hardware-induced windowing. The non-ideal properties of the lenses, the grating and beam shape cause an ellipse-shaped image of the interference pattern as shown in Fig. 9. Before applying an FFT on the measured patterns, pixel intensities of each column in the recorded image are summed and therefore the ellipse-shaped image results in an interference pattern in which the intensities are suppressed at the edges which means that it already consists of a certain window. Furthermore, it was seen that different optics resulted in change in artefacts. Therefore, it should be tested if larger lenses and grating can reduce the artefacts in the signals of ΔN_{eff}.

The analysis of an experiment with a two channel YI (two channels were blocked with a mask) showed similar artefacts as for a four channel YI, which means the artefacts are in the measured signal itself and not only induced by CT as there is only one spatial frequency peak for a two-channel YI.

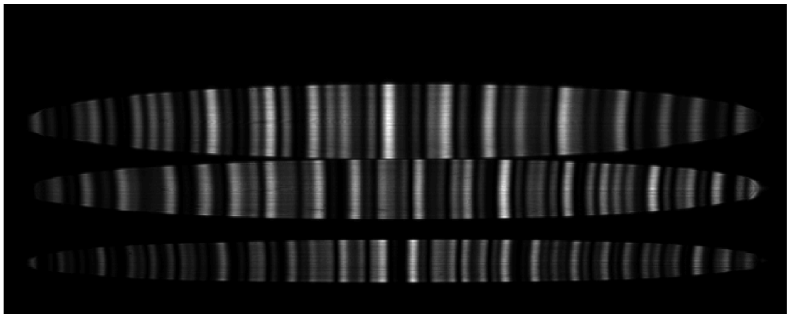

Fig. 9. Typical camera image illustrating three measured interference patterns from three different wavelengths, 660 nm, 561 nm and 457 nm, from top till bottom.

Appendix E. Influence of drift on determined RI change

Here, we show simulations that were done to determine the influence of drift in a measured signal of ΔN_{eff} on the result of Δn. For the determination of Δn, the matrix of the ratio-based analysis approach is used together with $R_{660/457}^{binding} = 0.919$, $R_{660/457}^{bulk} = 1.217$. The influence of linear drift in ΔN_{eff} on Δn is shown in Fig. 10. Linear drift in the signal ΔN_{eff} is translated to a linear drift in the result of Δn. The sign of the linear drift of Δn is the determined by the sign and ratio of the drift of ΔN_{eff} at the different wavelengths. This can be explained from a theoretical perspective:

$$\begin{bmatrix} \Delta n_1 \\ \Delta n_2 \end{bmatrix} = M \begin{bmatrix} \Delta N_{eff,1} + c_1 \cdot t \\ \Delta N_{eff,2} + c_2 \cdot t \end{bmatrix} = M \begin{bmatrix} \Delta N_{eff,1} \\ \Delta N_{eff,2} \end{bmatrix} + M \begin{bmatrix} c_1 \\ c_2 \end{bmatrix} t, \tag{9}$$

where c_1 and c_2 are constants which determine the amplitude of the linear drift of ΔN_{eff}. One can see that this finally results in linear drift in the signal of $\overline{\Delta n}$ which is determined by the coefficients of the matrix M and constants c_1 and c_2.

#257853 Received 5 Feb 2016; revised 14 Mar 2016; accepted 15 Mar 2016; published 12 Apr 2016

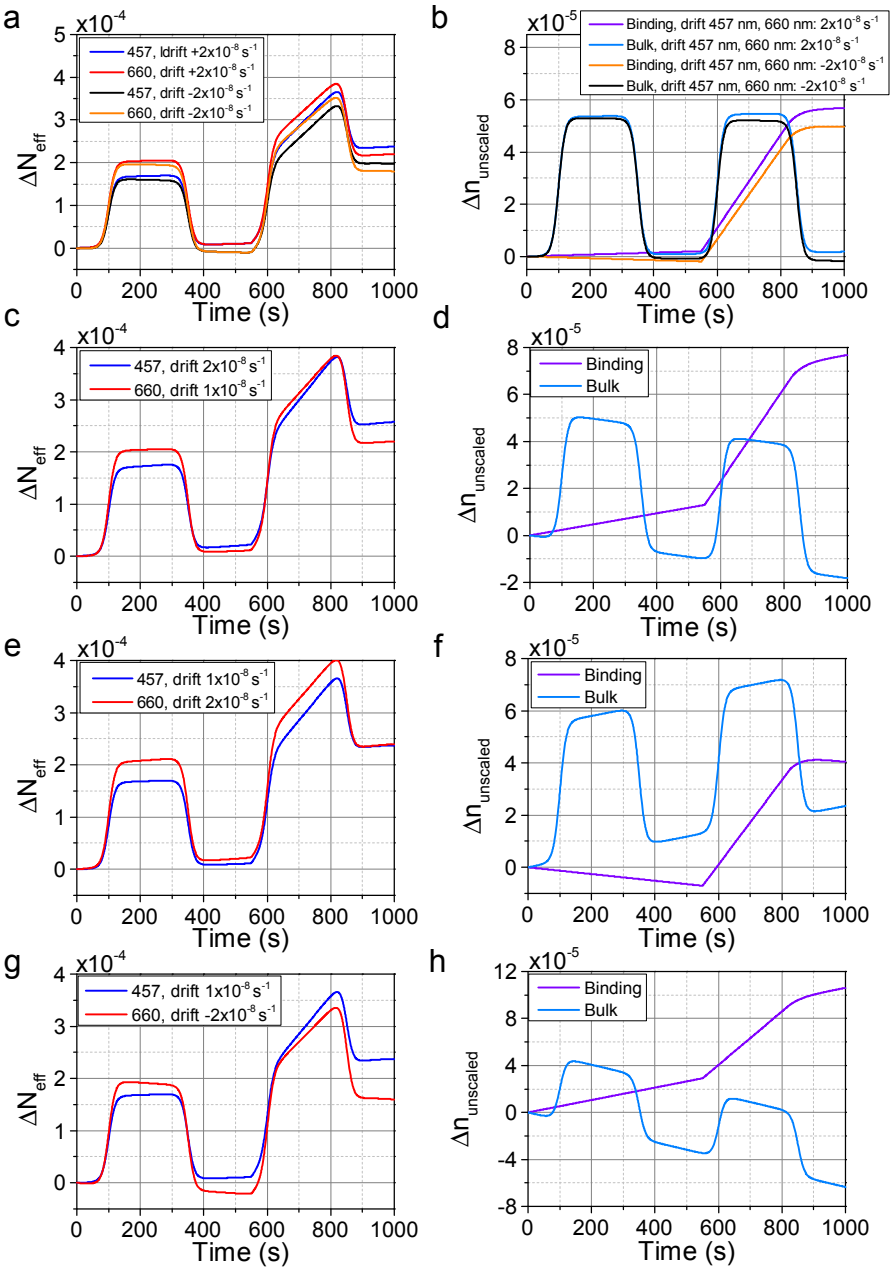

Fig. 10. a, c, e, g) A ΔN_{eff} over time with various added linear drifts and b, d, f, h) the corresponding determined $\Delta n_{unscaled}$ for binding and bulk signal, determined with ratio-based approach, illustrating that linear drift in ΔN_{eff} results is enhanced linear drift in $\Delta n_{unscaled}$.

Appendix F. Influence of input parameter values on the results for different analysis approaches

Calculating the value of Δn in the applied approaches depends on the values of the various input parameters needed for the different approaches. Here, we investigate the sensitivity of

#257853 Received 5 Feb 2016; revised 14 Mar 2016; accepted 15 Mar 2016; published 12 Apr 2016

the end-result on the parameter values. Figure 11 shows an experiment where first only D-glucose and later both 85 nm carboxylated polystyrene beads and D-glucose were added to the sensor, which is used for this investigation, and the corresponding determined Δn which the approach based on the approach based on the theoretical analysis and the ratio-based analysis approach.

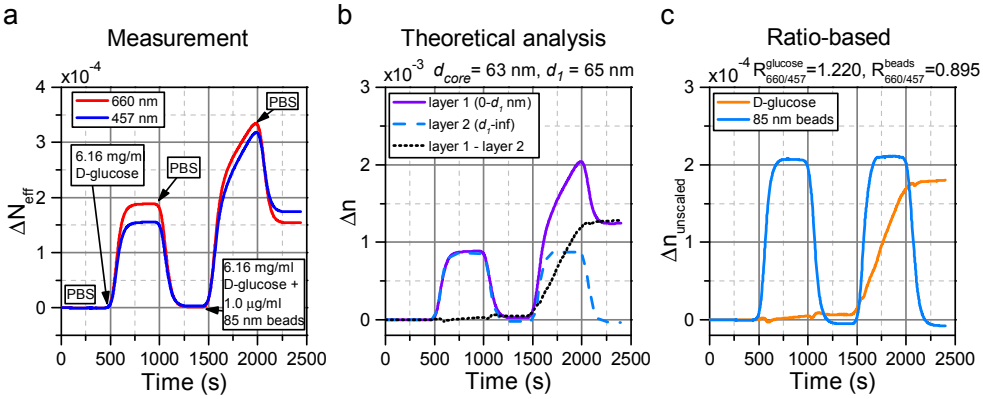

Fig. 11. Measurement where D-glucose and 85 nm beads are added to the sensor analysed with approach base on theoretical analysis and with ratio-based approach. a) Effective refractive index change over time at λ_1 = 457 nm and λ_2 = 660 nm for addition of 6.16 mg/ml D-glucose only and addition of 6.16 mg/ml D-glucose and 1.0 µg/ml 85 nm beads simultaneously, b) the determined Δn with the approach based on theoretical analysis and c) determined Δn with the ratio-based approach.

F.1 Approach based on theoretical analysis

The input parameters of the approach based on the theoretical analysis that were varied are d_{core} and d_1. Varying the d_{core} results in a varying level of both the value of Δn of layer 1 and layer 2 at the D-glucose step. Independent of the layer thickness d_1, the Δn at the addition of only D-glucose should be the same in both layers, which is realized by choosing d_{core} = 63 nm. Subsequently, the end level of both signals can be tuned by varying d_1. The end level of the bulk should be zero, because there was no Δn for the bulk compared to the starting situation were the bulk was also PBS. In the case of linear drift, the end level will not be zero but in line with the linear drift. This was realized with a d_1 = 65 nm, assuming a d_{core} = 63 nm. Figure 11(b) shows the optimal result for Δn based on d_{core} = 63 nm and d_1 = 65 nm. Next, the d_{core} and d_1 were varied and the change in $\Delta n_{l_1} - \Delta n_{l_2}$ (black dotted line in Fig. 11(b)) at t = 1900 s was determined. Consequently, the deviation in terms of percentage compared to the correct value of $\Delta n_{l_1} - \Delta n_{l_2}$ at t = 1900 s (based on d_{core} = 63 nm and d_1 = 65 nm) was determined, which is shown in Fig. 12. When we assume the deviation in $\Delta n_{l_1} - \Delta n_{l_2}$ should be maximally 10% and we fix the parameters d_{core} or d_1 and vary the other, this results in the dotted lines in Fig. 12. When both d_{core} and d_1 result in a deviation of 10% then the final deviation in $\Delta n_{l_1} - \Delta n_{l_2}$ stays within the 20%. We assume that this deviation is acceptable but off course the limits of the acceptable deviation might be different for each application. For the d_{core} this means that it should be determined with an maximal deviation of approximately ±1 nm. When this value is accurately determined it can be seen that the value of d_1 is less critical (a range of approximately 50 nm is fine). It should be noted that these deviations are determined for this specific case and at one time point. Deviations can be different when

#257853 Received 5 Feb 2016; revised 14 Mar 2016; accepted 15 Mar 2016; published 12 Apr 2016

substances are different. Moreover, deviations in terms of percentage might be much larger when $\Delta n_{l_1} - \Delta n_{l_2}$ goes towards zero.

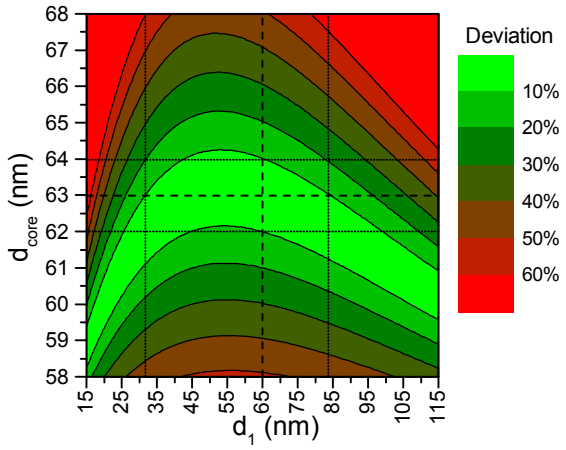

Fig. 12. Deviation in $\Delta n_{l_1} - \Delta n_{l_1}$ determined with the approach based on the theoretical analysis as a function of the input parameters d_{core} and d_1. The deviation in $\Delta n_{l_1} - \Delta n_{l_1}$ is given in terms of percentage and is determined compared to the correct value of $\Delta n_{l_1} - \Delta n_{l_1}$ based on d_{core} = 63 nm and d_1 = 65 nm which are represented by the dashed lines. The dotted lines show for which d_1 at the correct value of d_{core} (and *vice versa*) the $\Delta n_1 - \Delta n_2$ deviates 10% from the correct values.

F.2 Ratio-based approach

Here, we determined the influence of the ratios $R_{660/457}^{bead}$ and $R_{660/457}^{\text{glucose}}$ on the end result of Δn_{bead} and $\Delta n_{\text{glucose}}$. First, the best fit of Δn_{bead} and $\Delta n_{\text{glucose}}$ was determined. This resulted in a $R_{660/457}^{\text{glucose}}$ = 1.220, having a zero level for the beads when only D-glucose was added. To fit the end level of the D-glucose with the expected value, assuming a constant linear drift, the $R_{660/457}^{bead}$ = 0.895. Subsequently, the ratios $R_{660/457}^{bead}$ and $R_{660/457}^{\text{glucose}}$ were varied. The deviation of Δn_{bead} and $\Delta n_{\text{glucose}}$ (both at t = 1900 s) in terms of percentage compared with optimal fitted results are determined and shown in Fig. 13. When we assume a deviation in Δn_{bead} of maximally 10% for a fixed $R_{660/457}^{bead}$, the $R_{660/457}^{\text{glucose}}$ should be between 1.192 and 1.254 (see dotted lines in Fig. 13(a)). This results in an difference of 0.062 which is higher than the deviation measured in $R_{660/457}^{\text{glucose}}$ of 0.032 (= ±0.016, see Table 1), which means that the spread measured in $R_{660/457}^{\text{glucose}}$ results in acceptable deviation in Δn_{bead} based on the assumptions we made.

When we fix $R_{660/457}^{\text{glucose}}$ and assume again a maximal deviation of 10% in Δn_{bead}, the $R_{660/457}^{bead}$ should be between 0.859 and 0.925, which is equal to a difference of 0.066. When both ratios $R_{660/457}^{\text{glucose}}$ and $R_{660/457}^{bead}$ are varied with the deviation of 0.062 and 0.066 respectively, this result in a maximal deviation in Δn_{bead} of 20%. The difference of 0.066 is lower than the response of the beads between measurements of 0.090 (= ±0.045, see Table 1). So the spread measured in $R_{660/457}^{bead}$ is not acceptable when we assume a maximal deviation in Δn_{bead} of 20%. Therefore, more research is required to determine what the origin of the spread of the ratios is

#257853 Received 5 Feb 2016; revised 14 Mar 2016; accepted 15 Mar 2016; published 12 Apr 2016

in order to reduce this spread. It should be investigated if the spread can be explained by the artefacts or other noise sources of the measurements, the cleaning of the surfaces of the chip (larger spread is seen in binding of substances compared to bulk changes due to D-glucose) or the substances self (spread in protein A is smaller compared to beads). Again, it should be determined for each application what the maximally allowed deviation is and it should be noted these deviations are determined for this specific case and at one time point in the graph of Fig. 11.

The deviation of $\Delta n_{\text{glucose}}$ was also determined as a function of $R_{660/457}^{bead}$ and $R_{660/457}^{\text{glucose}}$ in a similar way as for Δn_{bead}. This resulted in comparable maximum allowable values of $R_{660/457}^{bead}$ and slightly higher maximum allowable values of $R_{660/457}^{\text{glucose}}$ as shown in Fig. 13(b). For determination of $\Delta n_{\text{glucose}}$ within 20% accuracy, the ratio $R_{660/457}^{\text{glucose}}$ should be between 1.181 and 1.271 and the ratio $R_{660/457}^{bead}$ should be between 0.857 and 0.926. These values correspond to spreads of 0.090 for $R_{660/457}^{\text{glucose}}$ and 0.069 for $R_{660/457}^{bead}$. Again, the spread in the measurements for $R_{660/457}^{\text{glucose}}$ from measurement to measurement is lower than the required 0.090, so sufficient. The spread in $R_{660/457}^{bead}$ from measurement to measurement is again higher than the required 0.069. Consequently, to determine the $\Delta n_{\text{glucose}}$ within 20% accuracy, the spread $R_{660/457}^{bead}$ from measurement to measurement should be reduced. As was stated before, more research is required to determine the origin of the spread.

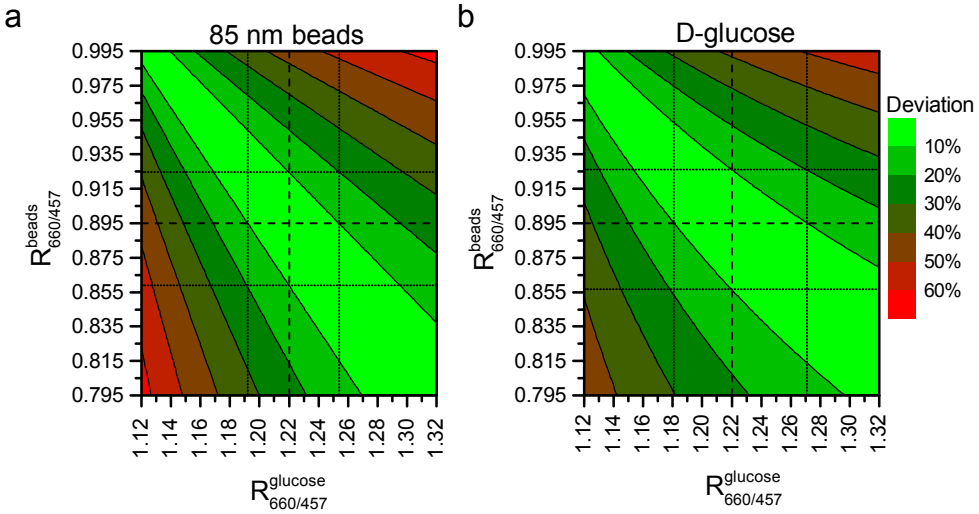

Fig. 13. Deviations in Δn_{bead} and $\Delta n_{\text{glucose}}$ determined with the ratio-based approach as a function of the input parameters $R_{\lambda_k/\lambda_l}^{\text{glucose}}$ and $R_{\lambda_k/\lambda_l}^{\text{bead}}$. The deviations in Δn_{bead} (a) and $\Delta n_{\text{glucose}}$ (b) are given in terms of percentage and is determined compared to the correct value of Δn_{bead} and $\Delta n_{\text{glucose}}$ respectively based on $R_{\lambda_k/\lambda_l}^{\text{glucose}}$ = 1.220 and $R_{\lambda_k/\lambda_l}^{\text{bead}}$ = 0.895 which are represented by the dashed lines. The dotted lines show for which $R_{\lambda_k/\lambda_l}^{\text{glucose}}$ at the correct value of $R_{\lambda_k/\lambda_l}^{\text{bead}}$ (and *vice versa*) the Δn_{bead} and $\Delta n_{\text{glucose}}$ deviate 10% from the correct values.

#257853 Received 5 Feb 2016; revised 14 Mar 2016; accepted 15 Mar 2016; published 12 Apr 2016

Appendix G. Cleaning protocol

As preferably the chip should be used in order to compare measurements, chips have to be reused and therefore cleaned sufficiently in between measurements. The following steps describe the cleaning procedure of the waveguide chips in between measurements:

1) rinse chip with water

2) rinse chip with acetone and wash chip with acetone and cotton (4x)

3) rinse chip with isopropanol (99.8%, filtered with 0.22 μm filter) and wash chip with same isopropanol and cotton (4x)

4) rinse chip with isopropanol (99.8%, filtered with 0.22 μm filter)

5) blow dry with instrumental air or nitrogen gas (N_2)

Fluorescent carboxylated beads were added to the sensor surface and after the measurement and after the cleaning protocol imaged with a fluorescence microscope to verify that the cleaning protocol was sufficient for removing the beads (see Fig. 14). As the protein A was not fluorescent and is smaller than the diffraction limit, the protein A could not be imaged and the cleaning protocol was not verified for the protein A. However, as we see that beads bind stronger to the surface than protein A (for protein A see more desorption after applying a washing step compared to the beads), we expect that the protein A is sufficiently removed from the surface using this cleaning protocol.

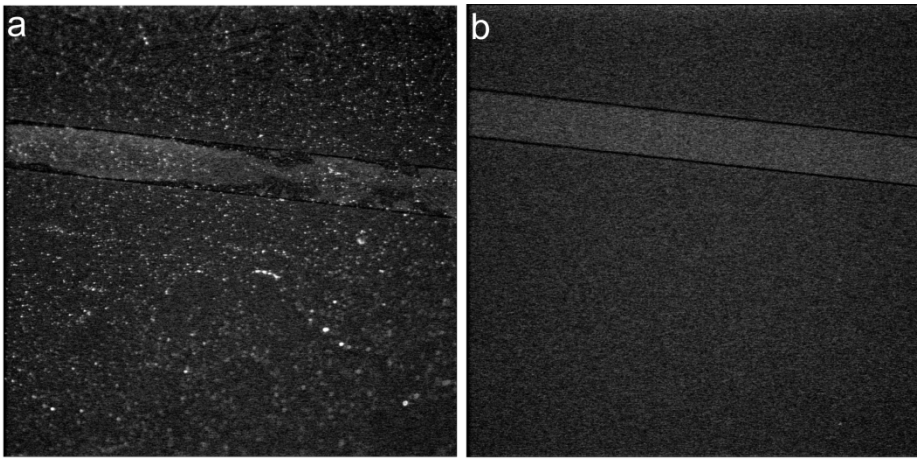

Fig. 14. Images of sensing windows after measurements with fluorescent beads a) before and b) after cleaning. Both images are taken with a 10x Plan Apo objective and an Andor DU-885 camera at an exposure time of 2 seconds and a multiplier of 80.

Acknowledgments

We want to thank XiO Photonics for their help with the realisation of the fiber butt-end coupling and A. Sidhu for her help in preparing the samples of the blind experiments. This work is supported by NanoNextNL, a micro and nanotechnology consortium of the Government of the Netherlands and 130 partners.